ADVANCES IN ATMOSPHERIC SCIENCES, VOL. 38, OCTOBER 2021, 1651–1664

• Original Paper •

Controls on the Northward Movement of the ITCZ over the South China Sea in Autumn: A Heavy Rain Case Study

Fei WANG[1,2], Lifang SHENG[*1,2,3], Xiadong AN[1], Qian LIU[4], Haixia ZHOU[5], Yingying ZHANG[6], and Jianping LI[7,8]

[1]*Department of Marine Meteorology*, *College of Oceanic and Atmospheric Sciences*, *Ocean University of China*, *Qingdao* 266100, *China*

[2]*Key Laboratory of South China Sea Meteorological Disaster Prevention and Mitigation of Hainan Province*, *Haikou* 570000, *China*

[3]*Ocean-Atmosphere Interaction and Climate Laboratory*, *Key Laboratory of Physical Oceanography*, *Ocean University of China*, *Qingdao* 266100, *China*

[4]*Department of Marine Meteorology*, *School of Atmospheric Sciences*, *Sun Yat-Sen University*, *Zhuhai* 519000, *China*

[5]*Sansha Meteorological Bureau of Hainan Province*, *Sansha* 573199, *China*

[6]*Professional Meteorological Science and Technology Service Center of Hainan province*, *Haikou* 570000, *China*

[7]*Frontiers Science Center for Deep Ocean Multispheres and Earth System (FDOMES)/Key Laboratory of Physical Oceanography/Institute for Advanced Ocean Studies*, *Ocean University of China*, *Qingdao* 266100, *China*

[8]*Laboratory for Ocean Dynamics and Climate*, *Pilot Qingdao National Laboratory for Marine Science and Technology*, *Qingdao* 266237, *China*

(Received 28 December 2020; revised 5 May 2021; accepted 12 May 2021)

ABSTRACT

The autumn Intertropical Convergence Zone (ITCZ) over the South China Sea (SCS) is typically held south of 10°N by prevailing northeasterly and weakening southwesterly winds. However, the ITCZ can move north, resulting in heavy rainfall in the northern SCS (NSCS). We investigate the mechanisms that drove the northward movement of the ITCZ and led to heavy non-tropical-cyclone rainfall over the NSCS in autumn of 2010. The results show that the rapid northward movement of the ITCZ on 1 and 2 October was caused by the joint influence of the equatorial easterlies (EE), southwesterly winds, and the easterly jet (EJ) in the NSCS. A high pressure center on the east side of Australia, strengthened by the quasi-biweekly oscillation and strong Walker circulation, was responsible for the EE to intensify and reach the SCS. The EE finally turned southeast and together with enhanced southwesterly winds associated with an anticyclone, pushed the ITCZ north. Meanwhile, the continental high moved east, which reduced the area of the EJ in the NSCS and made room for the ITCZ. Further regression analysis showed that the reduced area of the EJ and increased strength of the EE contributed significantly to the northward movement of the ITCZ. The enhancement of the EE preceded the northward movement of the ITCZ by six hours and pushed the ITCZ continually north. As the ITCZ approached 12°N, it not only transported warm moist air but also strengthened the dynamic field by transporting the positive vorticity horizontally and vertically which further contributed to the heavy rainfall.

Key words: ITCZ, rainfall, northern South China Sea, equatorial easterly, easterly jet

Citation: Wang, F., L. F. Sheng, X. D. An, Q. Liu, H. X. Zhou, Y. Y. Zhang, and J. P. Li., 2021: Controls on the northward movement of the ITCZ over the South China Sea in the autumn: A heavy rain case study. *Adv. Atmos. Sci.*, **38**(10), 1651–1664, https://doi.org/10.1007/s00376-021-0445-z.

Article Highlights:

- The equatorial easterlies, southwesterly winds, and the easterly jet in the NSCS jointly promoted the northward movement of the ITCZ in autumn of 2010.
- The enhancement of equatorial easterlies was related to the strengthened Walker circulation and an area of high pressure on the east side of Australia.
- 12°N was the appropriate position for ITCZ to influence the northern South China Sea.

* Corresponding author: Lifang SHENG
Email: shenglf@ouc.edu.cn

1. Introduction

Heavy rainfall over the South China Sea (SCS) occurs mainly in autumn, particularly in September and October, and accounts for 47.1% of the total annual rainfall in the area (Li et al., 2006). Xiao et al. (2013) found that the most intense autumn rainfall occurs over the SCS north of 10°N and southeast of Hainan Island. Previous research into the mechanisms of autumn rainfall over the SCS has focused mainly on the climatic scale or tropical cyclone (TC) precipitation at the synoptic scale (e.g., Wu et al., 2007; Shang et al., 2008). Some researchers have suggested that sea surface temperature (SST) anomalies in La Niña years induce an abnormal cyclone over the northern SCS (NSCS), and this increases precipitation (Feng et al., 2013; Li et al., 2015; Hu et al., 2020). However, 60% of the heavy rainfall over the SCS is non-tropical-cyclone (non-TC) precipitation of high intensity and long duration (Ren et al., 2006; Jiang and Zipser, 2010; Feng et al., 2017). Furthermore, the mechanism associated with this non-TC precipitation in the NSCS differs from that over southern China and Vietnam (Zhao et al., 2007; Niu and Li, 2008; Yokoi and Matsumoto, 2008; Yen et al., 2011; Gu et al., 2015).

The cold continental high (CH) and warm Intertropical Convergence Zone (ITCZ) are two of the many weather systems that affect the NSCS during autumn and are related mainly to heavy non-TC precipitation (Yen et al., 2011; Wang et al., 2015; Feng et al., 2017). For instance, when the ITCZ lies over the NSCS, it is possible for the warm and moist air it carries to mix with the cold air from the CH, resulting in a frontogenesis process and a commensurate increase in the gradient of the potential pseudo-equivalent temperature, both of which are beneficial to the generation of mesoscale convective weather (Yokoi and Matsumoto, 2008; Srock and Bosart, 2009). Meanwhile, the establishment of the low-level easterly jet (EJ) between the cold and warm systems usually induces instability (Liu et al., 2010; Feng et al., 2015), which also triggers heavy rainfall in the NSCS. In addition, Chang et al. (2005) found that the increased shear vorticity caused by the stronger northeasterly winds carried by the cold system contributes to the strengthening of the ITCZ and formation of a vortex, which also enhances precipitation generation. In contrast, in the absence of the ITCZ, heavy precipitation is suppressed. The ITCZ also brings about both low-level convergence (near 950 hPa) and high-level divergence (near 200 hPa) and is accompanied by the reinforcement of local positive vorticity advection and potential pseudo-equivalent temperature advection. This destroys the local quasi-geostrophic balance and aggravates the unstable stratification. The secondary circulation stimulated by the above dynamic forcing supports local ascent (Liu et al., 2010). The changes in temperature and humidity related to the dynamic process of the ITCZ are directly responsible for the rapid development of convection, leading to heavy rainfall (Wang and Magnusdottir, 2006; Li et al., 2009). In summary, the ITCZ plays a vital role in heavy non-TC rainfall over the NSCS. Consequently, two questions arise from these findings: how does the ITCZ move north into the NSCS during autumn, and what are the associated physical mechanisms?

The ITCZ position (P_{ITCZ}) in the SCS is closely related to the intensity of the winter or summer monsoon (Lander, 1996; Li and Ju, 2013) and the corresponding rain belt moves north-south seasonally (Hu et al., 2007; Xie et al., 2018). In summer, the ITCZ is pushed to around 20°N by the powerful southwesterly winds in the SCS, and the southwesterly flow on its south side facilitates the development of heavy rainfall over the NSCS and southern China (Zhao et al., 2007). In autumn, the southwesterly winds retreat and the northeasterly winds begin to play a role in the weather processes of the NSCS, also resulting in the southward movement of the ITCZ (Wei et al., 2008; Richter et al., 2017) and the southerly movement of the rain belt towards southern Vietnam (Yokoi et al., 2007; Yokoi and Matsumoto, 2008; Wang et al., 2015). Remarkably, however, under favorable conditions, the ITCZ in the SCS can move north to the appropriate position over 2–14 days (Lander, 1996; Magnusdottir and Wang, 2008; Chen et al., 2015) in autumn, where it can interact with a cold air mass from northern China, causing precipitation over the NSCS (i.e., the north side of the ITCZ) (Zhao et al., 2011; Xiao et al., 2013). Unfortunately, a detailed understanding of the mechanisms associated with this synoptic-scale northward movement of the ITCZ over the SCS, and the resultant heavy rainfall to its north, remains notably absent. So, it is hard to grasp when and where ITCZ begins to affect the NSCS, which leads to poor forecasting accuracy of non-TC autumn precipitation. This research is motivated by the above-mentioned questions, documents the heavy non-TC rainfall event over the NSCS in the autumn of 2010, and explores the mechanisms associated with the synoptic-scale northward movement of the ITCZ in the SCS.

The rest of the paper is organized as follows. Our data and methodology are described briefly in section 2. Section 3 quantitatively describes the northward movement of the ITCZ and the precipitation in the NSCS. The impact of the ITCZ on heavy rainfall is considered in section 4. The favorable factors that cause the northward movement of the ITCZ and the leading response of each factor to ITCZ movement are discussed in section 5. Section 6 presents the summary and discussion of our findings.

2. Data and methodology

2.1. *Data*

The Tropical Rainfall Measuring Mission level three product (TRMM_3B42RT) provided by the National Aeronautics and Space Administration (NASA) was used to describe rainfall over the NSCS (15°–20°N, 110°–120°E), at a temporal resolution of one day and a spatial resolution of 0.25° × 0.25° (Huffman et al., 2010). The FY2E satellite cloud images, obtained from the Institute for the Environment (IENV) at the Hong Kong University of Science and

Technology (HKUST), were used to analyze the changes in clouds during the ITCZ movement.

Reanalysis data including the meridional wind, zonal wind, geopotential height, air temperature, and specific humidity, at a temporal resolution of one hour and a spatial resolution of 0.5° × 0.5°, were obtained from the European Center for Medium-Range Weather Forecasts (ECMWF; Hersbach et al., 2020, hereafter referred to as ERA5) to determine P_{ITCZ} and investigate the associated atmospheric circulation. In addition, interpolated outing longwave radiation (OLR) data with a temporal resolution of one day and a spatial resolution of 2.5° × 2.5°, provided by the National Oceanic and Atmospheric Administration (NOAA; Liebman and Smith, 1996), were used to calculate the ITCZ intensity. Monthly mean Niño-3 index and SST data for the Niño-3 area (5°S–5°N, 150°–90°W), derived from the Extended Reconstructed Sea Surface Temperature Version 5 (ERSSTv5; Huang et al., 2017) dataset and provided by the Climate Prediction Center (CPC), were used to demonstrate the favorable SST variations that promoted the northward movement of the ITCZ.

2.2. *Methods*

We defined the value of P_{ITCZ} in the SCS as the position of the eastward (west to east) wind shear line at 850 hPa, as shown in Fig. 1. To filter out the high-frequency waves (less than three days), the zonal wind data used to calculate P_{ITCZ} were obtained via low-pass filtering of the raw data. The SCS region (0°–24°N, 110°–120°E) was divided into 24 × 19 grid cells, with a meridional and zonal resolution of 0.5° and 1°, respectively. We determined the direction (D) using the following equation:

$$D = \bar{u}_l \times \bar{u}_h \,, \tag{1}$$

where $\bar{u}_l$ and $\bar{u}_h$ represent the zonal wind in a low-latitude and high-latitude grid cell, respectively, and D indicates the wind direction. If $\bar{u}_l > 0$ and $D < 0$, then there are westerly winds in the low-latitude grid cell and easterly winds in the high-latitude grid cell. The point between the two grid cells was defined as a point lying on the central axis of the ITCZ.

We used the following method to eliminate the abnormal points and select the eligible points:

$$P' = P - \overline{P} \,, \tag{2}$$

here, P is the latitude of the point selected according to equation (1), $\overline{P}$ is the average of all P values, and P' is the difference between P and $\overline{P}$. If $P' > 5°$, P was considered to be an abnormal point and eliminated. If the number of selected points was greater than three in any one day, then we concluded that the SCS was being influenced by the ITCZ. The P_{ITCZ} index (PI_{ITCZ}) was defined as the average latitude of all eligible P values. Hereafter, all future references to the ITCZ refer to the ITCZ in the SCS.

In addition to the method outlined above, OLR data are often used to quantitatively describe the features of the ITCZ (Zhang and Jiang, 2001; Meenu et al., 2007). In this study, the intensity of the ITCZ was characterized as follows:

$$II_{ITCZ} = M_{(PI_{ITCZ}-5, PI_{ITCZ}+5)} \,, \tag{3}$$

where M is the minimum OLR value, II_{ITCZ} represents the ITCZ intensity index and is the minimum OLR value within 5° of latitude north and south of the PI_{ITCZ}; i.e., the smaller the OLR value, the stronger the ITCZ intensity.

Tropical Cyclone (TC) precipitation in the SCS falls mainly within 2.5° of longitude from the TC center (Chen et al., 2010; Feng et al., 2013); consequently, TCs with a center west of 130°E or south of 30°N can affect the NSCS. We eliminated dates on which TCs influenced the NSCS based on TC path data provided by the Japan Meteorological Agency, and found that a non-TC precipitation event occurred between 29 September and 5 October 2010 over the NSCS.

3. Northward movement of the ITCZ and resultant rainfall in the NSCS

During the non-TC precipitation event between 29

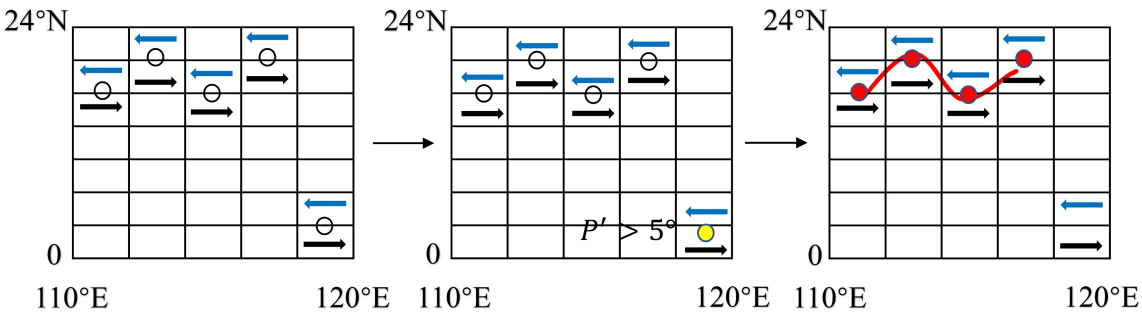

Fig. 1. Schematic representation of the definition of P_{ITCZ}. The three large boxes represent the area covered by the SCS (0°–24°N, 110°–120°E), which were divided into 24 × 19 grid cells. The first box shows all positions where $\bar{u}_l > 0$ and $D < 0$, the second is quality control for P, and the third shows the distribution of the ITCZ. Black and blue arrows represent westerly and easterly winds, respectively. The black circles indicate the central position where the wind shear occurs, the yellow solid circle is the abnormal point, and the red solid circles are the points along the central axis of the ITCZ.

September and 5 October 2010, the ITCZ moved northward from 8.3°N to 17.6°N. Cloud images and OLR data also demonstrated this process (not shown). We divided this process into three stages based on the speed of the ITCZ movement (Fig. 2). The northerly progress of the ITCZ was slowest (about 0.8° per day) from 29 September to 1 October, and fastest (about 2.5° per day) between 1 and 2 October, showing a sudden increase in intensity (Fig. 2). Subsequently, the ITCZ continued to move north at a moderate rate of 1.7° per day from 2 to 5 October. There was an east-west cloud band on the south side of the ITCZ when it was located south of 10°N (Fig. 3a). When the ITCZ moved to 12.3°N on 2 October, there were two cloud bands on both

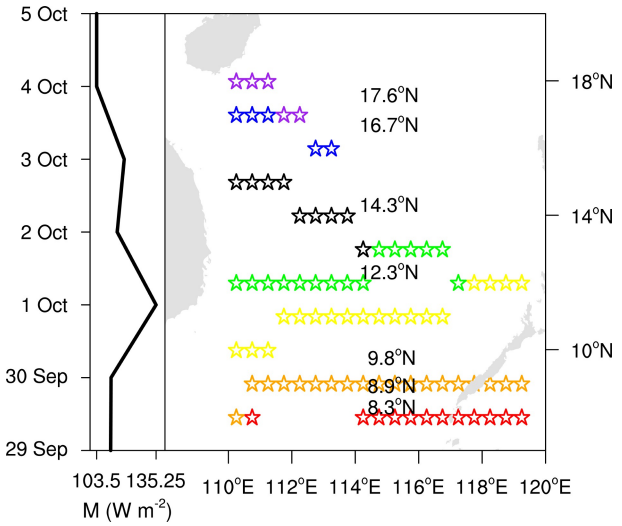

Fig. 2. The distribution of P_{ITCZ} (right) and M (the minimum OLR value) variation over time (left; units: W m^{-2}). The red, orange, yellow, green, black, blue, and purple stars (and accompanying numbers) indicate the PI_{ITCZ} from 29 September to 5 October 2010, respectively.

the northern and southern sides of the ITCZ (Fig. 3b), which indicates that the ITCZ had begun to interact with the mid-latitude weather systems, and this interaction coincided with the rainfall over the NSCS. For quality control, we compared the ERA5 results with results obtained from The National Centers for Environmental Prediction (NCEP) reanalysis (Kalnay et al., 1996). The calculation error of the two sets of datasets on the PI_{ITCZ} was ~1.2°. However, both datasets revealed that the most obvious northward movement of the ITCZ occurred on 1–2 October During this time, the ITCZ began to influence the NSCS as it approached near 12°N, and moved faster after the rain than before.

Over the period 2–5 October 2010, the accumulated rainfall broke the record that had stood since 1970 in the NSCS. The rain around Hainan Island began on 2 October, with a daily area-averaged rainfall (15°–20°N, 110°–120°E) of 21.3 mm, with rainfall occurring in 445 grid cells (Fig. 4d). Subsequently, the number of grid cells with rainfall decreased slightly, but the daily area-averaged rainfall increased significantly and it reached its maximum value of 33.4 mm on 5 October (Figs. 4e and 4f). The development of this rainfall was closely related to the ITCZ. When the ITCZ was south of 10°N, the rainfall was weak and scattered near the ITCZ (Figs. 4a and 4b). The rainfall over the NSCS concentrated significantly towards Hainan Island and the surrounding sea area commensurate with the strengthening and northwestward movement of the ITCZ (Figs. 4c–4f).

4. Ingredients for heavy rainfall caused by the ITCZ

4.1. *Moisture was transported by the ITCZ*

An abundant supply of moisture is one of the condi-

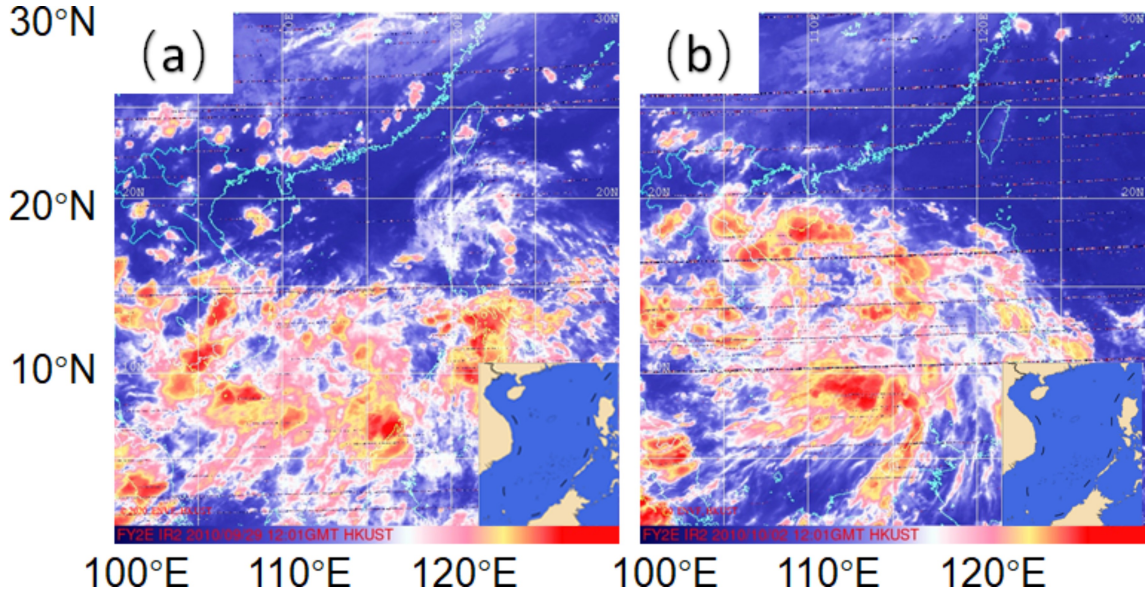

Fig. 3. Cloud images from (a) before (1200 UTC 29 September 2010) and (b) after (1200 UTC 2 October 2010) the heavy rainfall in the NSCS.

tions required for the generation of heavy rainfall. We determined the source of moisture over the NSCS by calculating the integral of the water vapor flux (WVF) at 1000–300 hPa based on the method applied by Fasullo and Webster (2003). Figure 5a shows that the moisture over the NSCS before the period of heavy rainfall came mainly from the western Pacific. The maximum WVF value was ~ 400 kg m^{-1} s^{-1} and concentrated below 900 hPa (Fig. 6a). When the ITCZ approached 12°N on 2 October, moisture was transported by the southwesterly winds on the south side of the ITCZ into the NSCS from the Bay of Bengal and the western Pacific, which, together, enhanced the WVF in the NSCS (Fig. 5b). In the meantime, more moisture extended vertically to 500 hPa (Fig. 6b) and the heavy rainfall began in the NSCS. As the ITCZ entered the NSCS, the moisture from the Bay of Bengal was dominant (Fig. 5c) and continued to spread vertically (Fig. 6c), which intensified the rainfall. We concluded that the moisture supplied from the Bay of Bengal that was driven by the northward movement of the ITCZ, constituted the primary source of the moisture that caused the rainfall in the NSCS.

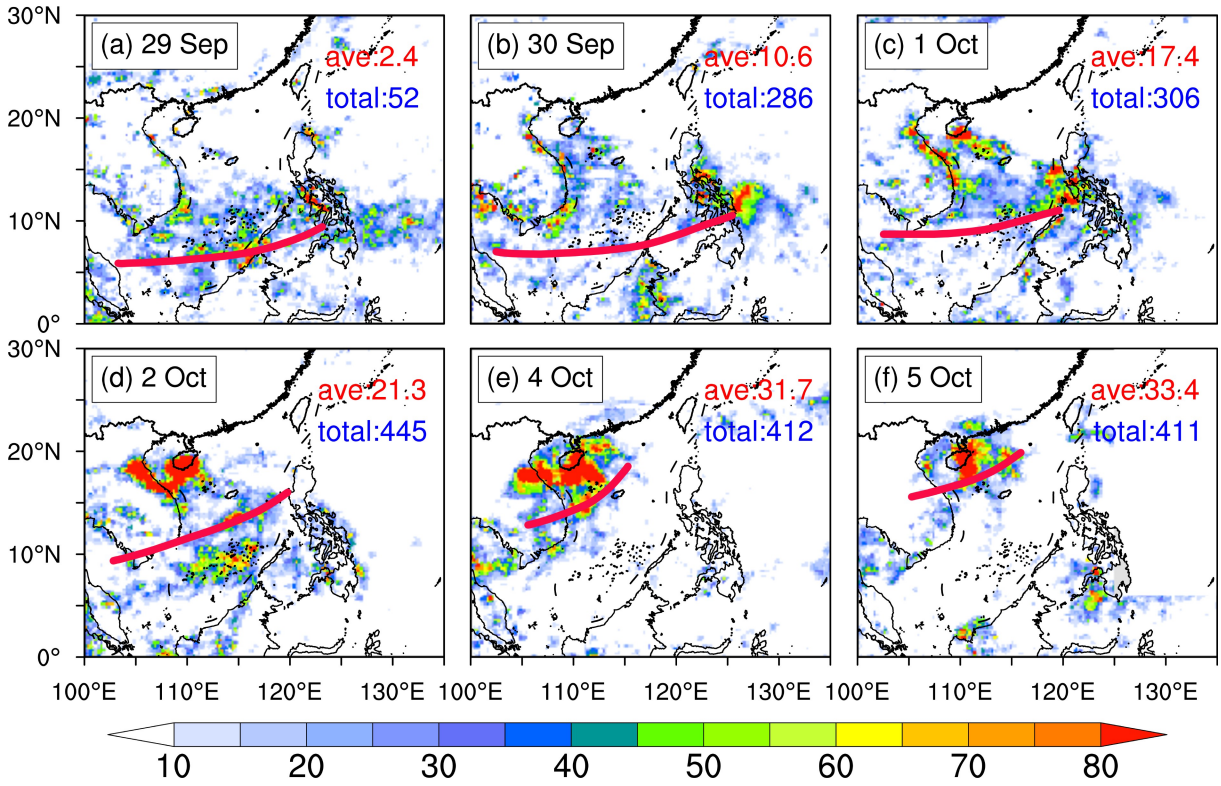

Fig. 4. Spatial distribution of P_{ITCZ} (red solid line) and daily rainfall (shading; units: mm) in the SCS area. (a)–(f) shows plots for 29 and 30 September, and 1, 2, 4, and 5 October 2010, respectively. The red and blue text indicates the daily area-averaged rainfall and the number of grid cells with rainfall in the NSCS (15°–20°N, 110°–120°E), respectively.

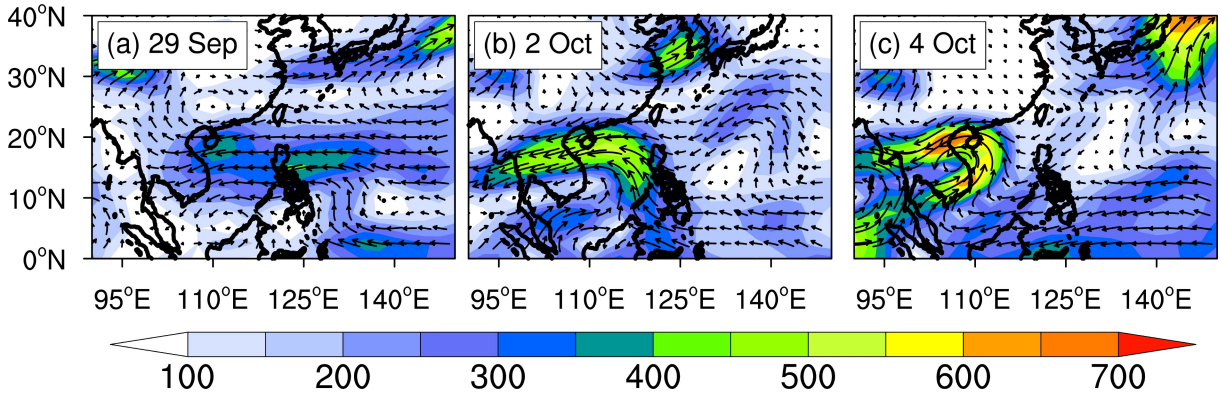

Fig. 5. Integrated WVF from 1000 to 300 hPa (units: kg m^{-1} s^{-1}) for (a)–(c) 29 September (before rainfall), 2 October (start of rainfall), and 4 October (during rainfall) 2010, respectively. The shading and arrows represent the WVF value and vector, respectively.

4.2. *Atmospheric instability and ascending motion were strengthened by the ITCZ*

In addition to moisture supply, the atmospheric instability and strong ascending motion also facilitated the generation of heavy rainfall. We calculated the tropospheric stability based on the temperature difference between the middle and lower levels (Liu et al., 2017) as follows:

$$\Delta\theta_{se} = \theta_{se(500)} - \theta_{se(850)}\,, \tag{4}$$

here, $\theta_{se(500)}$ and $\theta_{se(850)}$ are the pseudo-equivalent potential temperature (θ_{se}) at 500 hPa and 850 hPa, respectively. $\Delta\theta_{se}$ is the instability criterion. When $\Delta\theta_{se} < 0$, the atmosphere is unstable. As shown in Figs. 6a and 6b, $\Delta\theta_{se}$ changed from −2.5 K on 29 September to −6.3 K on 2 October, and there was a noticeable θ_{se} tongue near 115°E associated with the vertical expansion of moisture (Fig. 6b). This suggests that the atmosphere became unstable in the NSCS when the ITCZ moved to around 12°N on 2 October. At this time, the atmospheric instability was related to the convergence of warm and cold advection carried by the ITCZ and CH, respectively (not shown). As the ITCZ entered the NSCS, the warm air accumulated in the NSCS, thereby decreasing the temperature gradient. As a result, the θ_{se} tongue gradually disappeared. However, the ITCZ strengthened the dynamic field to support the vertical expansion of moisture and maintain the precipitation (Fig. 6c).

For the dynamic field in the NSCS, when the ITCZ arrived at around 12°N, the positive vorticity, the low-level convergence, and ascending motions were obviously stronger than before (Figs. 7a and 7b). This, together with sufficient moisture and atmospheric instability, generated the heavy rainfall. As the ITCZ covered the NSCS, the low-level convergence strengthened further and was accompanied by a more violent ascending motion. This enhancement of the convergence and ascending motion was related to the strengthening and thickening of the positive vorticity layer (Figs. 7b and 7c). To further assess the impact of the ITCZ on the development of the positive vorticity in the NSCS, we used the vorticity budget equation (Chen and Zheng, 2004; Nguyen and Molinari, 2015) as follows:

$$\frac{\partial\zeta}{\partial t} = -\left[u\frac{\partial\zeta}{\partial x} + v\frac{\partial}{\partial y}(\zeta+f)\right] - \omega\frac{\partial\zeta}{\partial p} - (\zeta+f)\nabla\cdot\boldsymbol{V} - \left(\frac{\partial\omega}{\partial x}\frac{\partial v}{\partial p} - \frac{\partial\omega}{\partial y}\frac{\partial u}{\partial p}\right), \tag{5}$$

here, ζ is the relative vorticity, $\boldsymbol{V}$ is the horizontal velocity vector, f is the Coriolis parameter, and u, v, and ω are the three-dimensional flow components. The terms on the right-hand side of Eq. (5) in turn are the horizontal advection of absolute vorticity, the vertical advection of absolute vorticity, stretching of absolute vorticity, and tilting of horizontal vorticity into the vertical. We ignored the friction term in this study because of its insignificant contribution.

We found that the enhancement of positive vorticity below 500 hPa was associated mainly with the horizontal advection and stretching terms on 2 October (Fig. 7e). This enhancement was a consequence of the horizontal transport of positive vorticity to the NSCS by the ITCZ as it approached 12°N. Subsequently, the vertical advection and stretching terms made a positive contribution to the strengthening and thickening of the positive vorticity layer (Fig. 7f). The positive vorticity layer was further thickened to 300 hPa, and the positive vorticity around 700–500 hPa increased significantly (Figs. 7c and 7f). At this time, the ITCZ controlled the NSCS, which was why the positive vorticity was transported vertically to middle levels. This was conducive to the enhancement of the dynamic field of precipitation.

5. The factors responsible for the northward movement of the ITCZ

In this section, we explore the mechanisms that cause

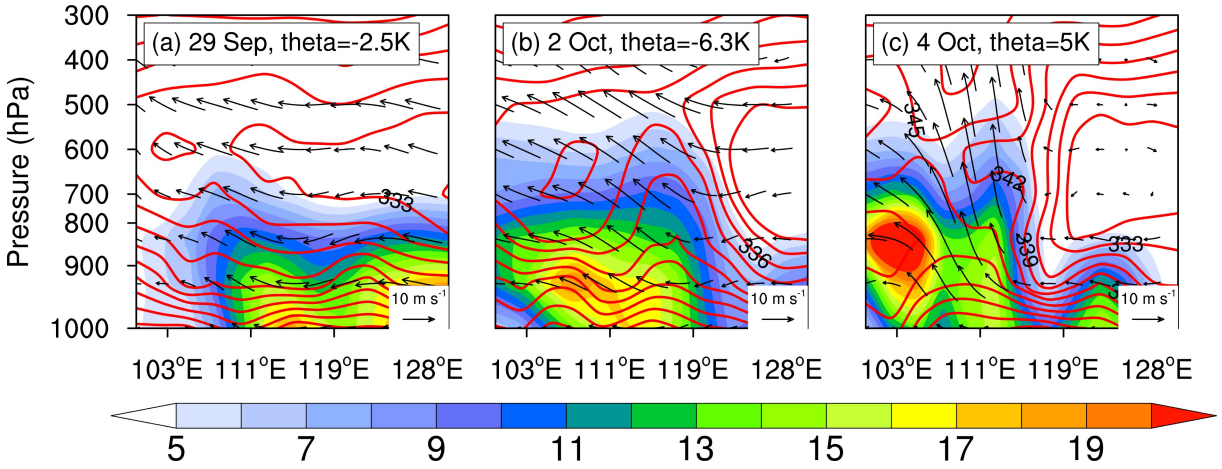

Fig. 6. Vertical cross-section of the WVF (shading; units: kg m^{-1}s^{-1}), pseudo-equivalent potential temperature (red contours, interval: 3 K) and wind (zonal wind and omega, arrows; units: m s^{-1}) along 18.5°N, and black texts for $\Delta\theta_{se}$. The periods covered by (a)–(c) are the same as in Fig. 5.

the northward movement of the ITCZ. Figure 8 shows the correlation coefficient between PI_{ITCZ} and wind speed at 850 hPa using hourly data. The southwesterly and southeasterly winds on the south side of the ITCZ were favorable to the northward movement of the ITCZ, whereas the easterly winds on the north side of the ITCZ had the opposite effect (Fig. 8). The southwesterly flow originates mainly from the Somalian cross-equatorial airflow and the cross-equatorial airflow near 105°E. The southeasterly flow is formed as the equatorial easterlies (EE) turn upon reaching the SCS, The easterly wind flows into the NSCS from the south of a mid-latitude high pressure system.

5.1. *Equatorial easterly promoted the ITCZ move north*

We will first examine the effect of the strengthened EE on the northward movement of the ITCZ. In section three, we divided the northward movement of the ITCZ into three stages. Figures 9a–c show the average wind field during

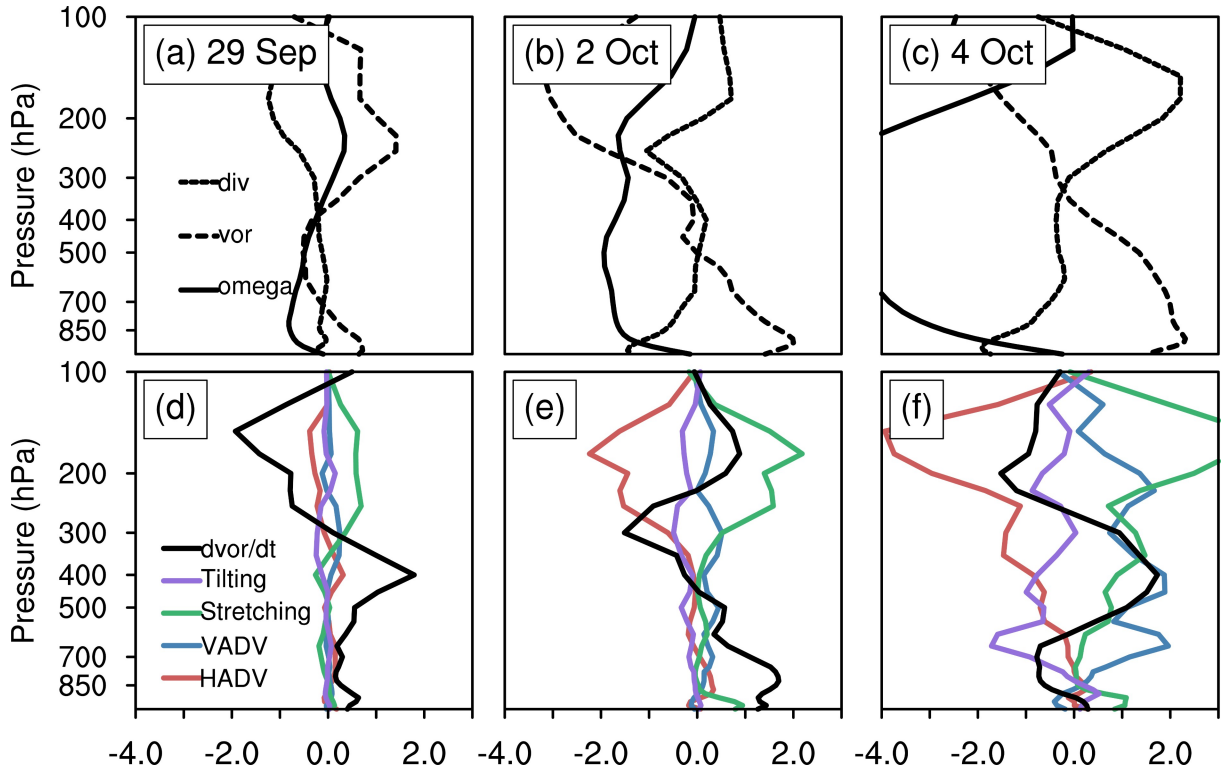

Fig. 7. (a)–(c) Profiles of average divergence (dotted; units: 10^{-5} s^{-1}), convergence (dashed; units: 10^{-5} s^{-1}), and omega (solid; units: 10^{-1} Pa s^{-1}) in the NSCS. (d)–(f) Profiles of the average contribution to the relative vorticity tendency (units: 10^{-9} s^{-2}) from horizontal advection (red), vertical advection (blue), tilting (purple), and stretching (green) for the NSCS. Periods covered by (a)–(c) and (d)–(f) are the same as in Fig. 5.

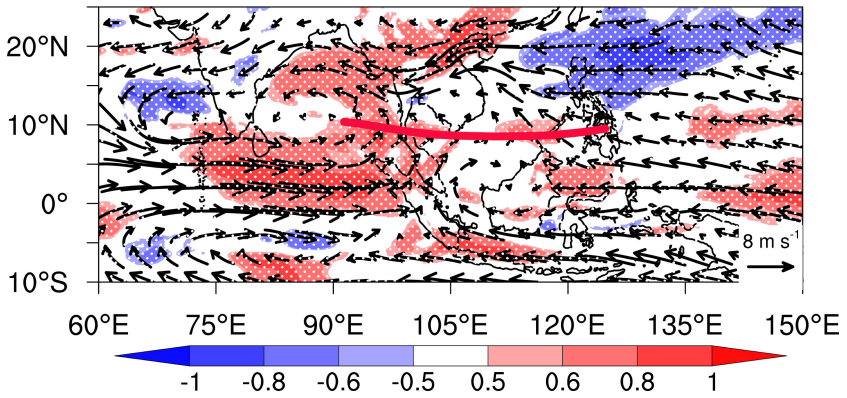

Fig. 8. The correlation between P_{ITCZ} and wind speed at 850 hPa (shading, only those regions where the correlation coefficient is greater than 0.4 and passes 95% significance using the Student's *t*-test are shaded) and average wind speed at 850 hPa (arrows; units: m s^{-1}) between 29 September and 5 October 2010. The red line indicates the average distribution of P_{ITCZ}.

these three stages, and Fig. 9d shows the variation of the average wind over time within 5° of latitude on the south side of the ITCZ. Between 29 September and 1 October, the ITCZ south of 10°N was pushed slowly northward at an average speed of 0.8° per day by southwesterly winds (Figs. 9c and 9d). On 1–2 October, the southwesterly wind was strengthened by an equatorial anticyclone (the negative vorticity attained a maximum in the area 110°–120°E, 5°S–5°N, shown in the red box of Fig. 9b on 1 October), and the EE reached the SCS and then turned to the southeast. The two flows merged to form a strong southerly wind, which enabled the ITCZ to move quickly north (at about 2.5° per day) and reach the vicinity of 12°N (Figs. 9b, d). However, the anticyclone was short-lived (the negative vorticity gradually decreased); consequently, the action time of the southwesterly wind on the northward movement of the ITCZ was also short. Hereafter, the EE continued to pour into the SCS and turned into the southeasterly wind, pushing the ITCZ northwest at an average speed of 1.7° per day during 2–5 October (Figs. 9a, 9d). From the above analysis, the southwesterly wind played only a temporary role in the northward movement of the ITCZ. Therefore, we propose that the EE were more important in driving the ITCZ northward consistently over this period.

Regarding the strengthening of EE, we explored the contribution of the SST in the Pacific to EE enhancement. We found that a La Niña event developed in 2010 (Gu et al., 2015), and the Niño 3 index and the SST in the Niño-3 region dropped to a minimum in October (not shown). Additionally, the variation of the weekly data further demonstrated that the SST in the Niño- 3 region during this process decreased from its value of the previous week (Fig. 10a). This resulted in further intensification of the Walker circulation as a result of this process (Feng et al., 2013; Chiodi and Harrison, 2015; Hu et al., 2020), which enhanced the EE, enabling it to reach the SCS to support the northward movement of the ITCZ (Fig. 10b).

Four heavy rainfall events in the NSCS resulted from this kind of ITCZ movement over the periods 8–13 October 2008, 9–15 September 2011, 7–13 September 2013, and 6–9 October 2017 during 2008–17. Notably, all episodes occurred in La Niña years. This further suggests that the La

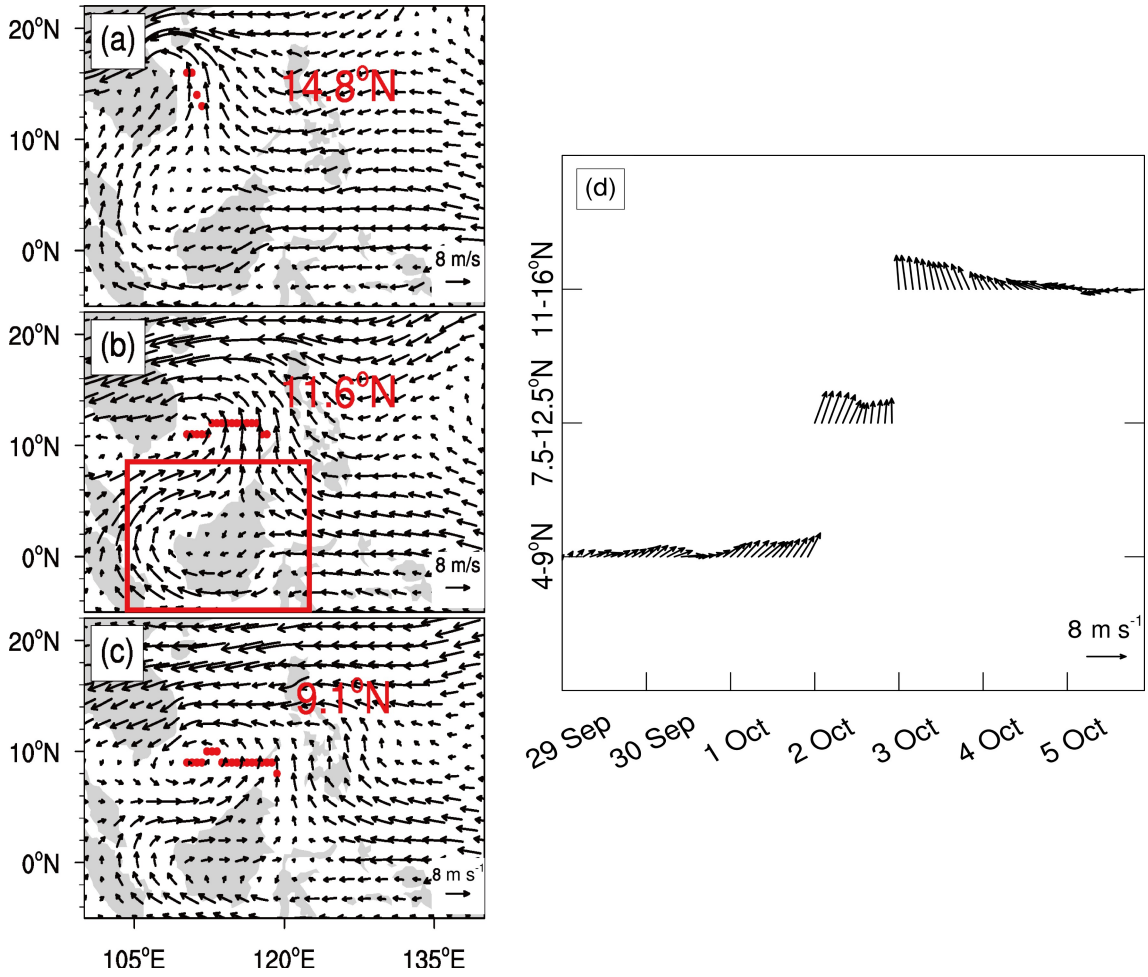

Fig. 9. (a)–(c) The average wind (units: m s^{-1}) at 850 hPa during 2–5 October, 1–2 October, and 29 September to 1 October 2010, respectively. Red dots are the distribution of P_{ITCZ}. Red numbers are the average values of P_{ITCZ}. The red box shows the location of the equatorial anticyclone. (d) Variation of the average wind (units: m s^{-1}) within 5° of latitude on the south side of the ITCZ over time.

Niña events are conducive to the strengthening of the EE, which may help the ITCZ to move north, finally causing heavy rainfall over the NSCS in autumn.

In addition to the impact of the SST on the EE, we found that the average wind speed within the region 0°–10°N, 120°–180°E (black box in Fig. 11) corresponding to the EE showed a strong positive correlation with the Mascarene High, the western Pacific subtropical high (WPSH; Bian et al., 2018), and the high on the east side of Australia, which is evident from the geopotential height field at 850 hPa (Fig. 11). The intensity of the Mascarene High changed little during the northward movement of the ITCZ (Fig. 12a). The high on the east side of Australia might have played a vital role in strengthening the EE, noting that it had strengthened since 30 September, 2010 (Fig. 12a) due to the eastward propagation of the quasi-biweekly oscillation near 30°S (Fig. 12b). Zhou and Cui (2011) found that higher SSTs on the east side of Australia are instru-

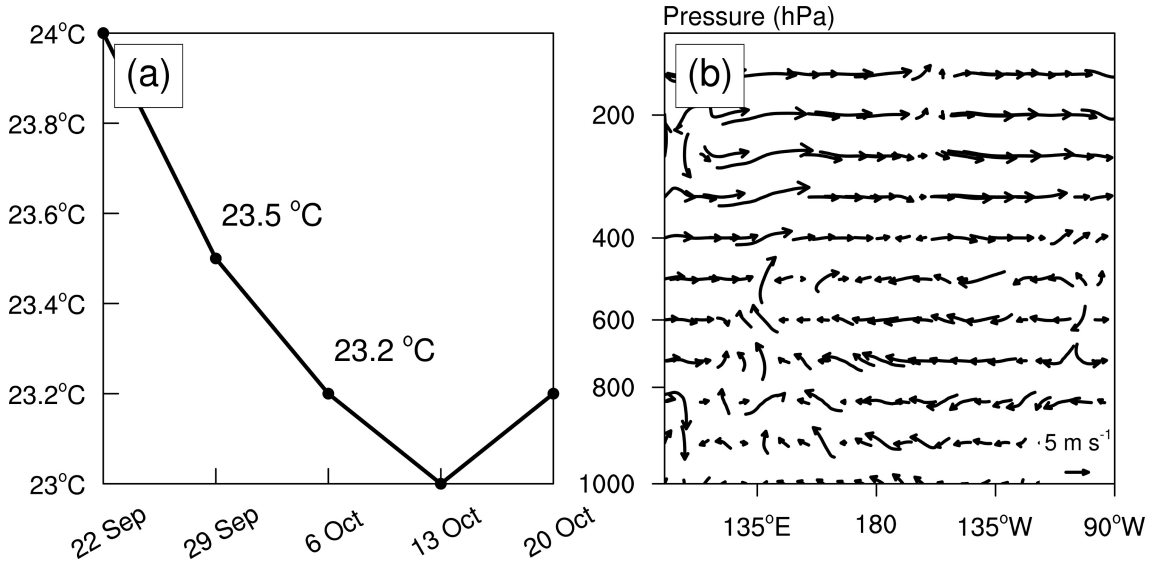

Fig. 10. (a) The variation of the weekly averaged SST (black; units: °C) in the Niño-3 region from 22 September to 20 October 2010. (b) A vertical cross-section in 0°–5°S of the wind difference (arrows; units: m s^{-1}) between 22–29 September and 29 September–6 October 2010.

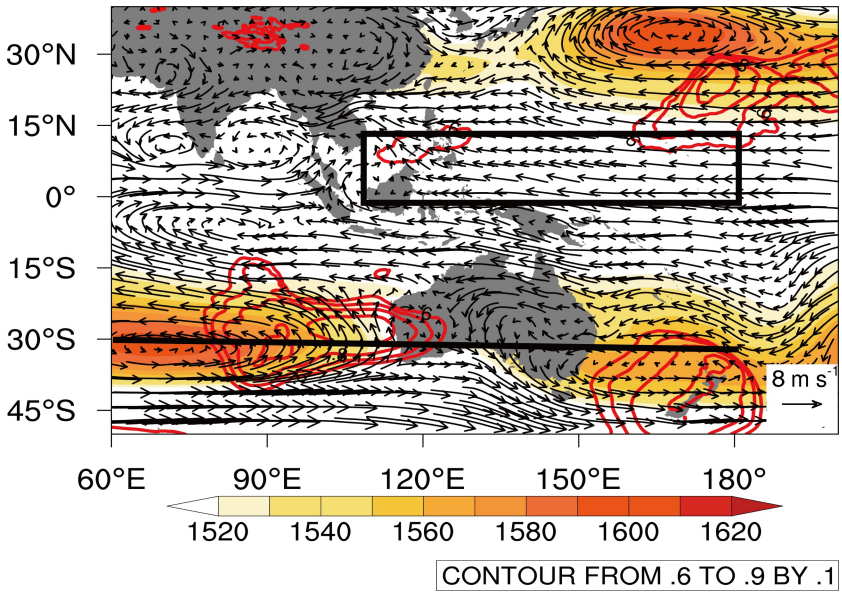

Fig. 11. Average wind speed (arrows; units: m s^{-1}) and geopotential height (shading, only values greater than 1520 are shown; units: gpm) at 850 hPa from 29 September to 5 October 2010, and the correlation coefficient between the area-averaged wind speed across the area bounded by 0°–10°N, 120°–180°E (black box) and geopotential height (red contours, only those regions where the correlation coefficient is greater than 0.6 and passes 95% significance using the Student's *t*-test are shown). The black line marks the transect used to draw the Hovmöller diagrams.

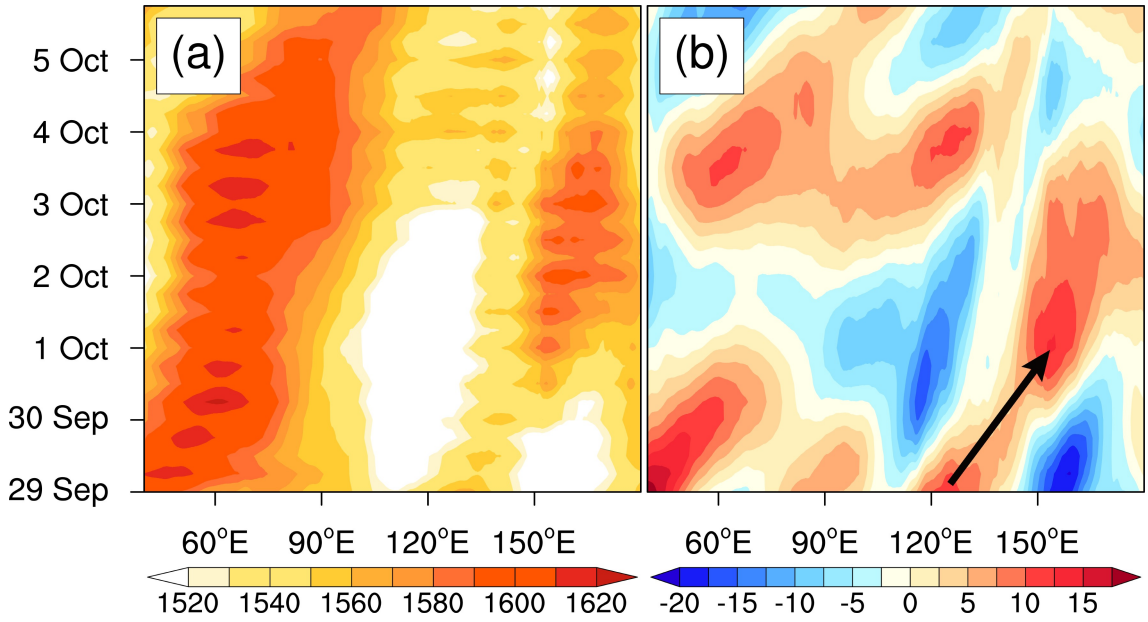

Fig. 12. (a) Hovmöller diagram of geopotential height (units: gpm), and (b) the quasi-biweekly oscillation (i.e., the 10- to 20-day filtered geopotential height) at 850 hPa along 30°S (black line in Fig. 11). The black arrow indicates the eastward propagation of the quasi-biweekly oscillation.

mental in developing the geopotential height here and an abnormal EE. Therefore, the positive SST anomaly on the east side of Australia, typically present in La Niña years, may be more favorable to the positive geopotential height and an EE anomaly.

5.2. *The easterly jet in the NSCS made room for the northward movement of ITCZ*

Apart from the EE, the decrease in the area influenced by the EJ over the NSCS also plays an important role in the northward movement of the ITCZ. As shown in Fig.13a, easterly flow from the combined CH and WPSH induced the EJ on the north side of the ITCZ, which is key to triggering heavy rainfall over the NSCS (Liu et al., 2010; Feng et al., 2015). However, the EJ also inhibits the northward movement of the ITCZ (Fig. 8), which is not conducive to the maintenance of heavy rainfall. On 1–2 October, the temperature, and vorticity gradients at 850 hPa over the NSCS decreased significantly owing to the reduction of geopotential height at 850 hPa between 110°–140°E by the CH moving to the east of 140°E and merging into the WPSH, which weakened the EJ (Sreekala et al., 2014; Feng et al., 2015; Figs. 13b and 13c). As a result, the ITCZ moved rapidly north (Fig. 2). Later, the local EJ increased due to the southward movement of a new CH (Fig. 13d) and the northward movement of the ITCZ also slowed (Fig. 2).

To further investigate the relationship between the EJ in the NSCS and PI_{ITCZ}, we calculated the correlation coefficient between the index of the EJ area (AI_{EJ}) and intensity (II_{EJ}) and the PI_{ITCZ}. The number of grid points with a wind speed at 850 hPa greater than 10 m s^{-1} over the NSCS (15°–20°N, 110°–120°E) was defined as the AI_{EJ}, and an average speed of more than 10 m s^{-1} was recorded as II_{EJ}. The correlation coefficient between PI_{ITCZ} and AI_{EJ} was −0.61 (above the 95% confidence level), whereas the correlation coefficient between PI_{ITCZ} and II_{EJ} was small. Therefore, the eastward movement of the CH and its subsequent merger into the WPSH at 850 hPa resulted in a decrease in the area of the EJ over the NSCS, which was conducive to the northward movement of the ITCZ. In contrast, the southerly movement of the new CH increased the area of the local EJ, and this limited the northward movement of the ITCZ during the third stage.

We also used multiple linear regression analysis between PI_{ITCZ} and the AI_{EJ}, the southwesterly index (SWI), and the EE index (EEI) to further assess the contribution of each factor to P_{ITCZ}. The average zonal wind speeds in the regions 0°–10°N, 90°–110°E, and 0°–10°N, 120°–140°E were used to define the SWI and EEI indices, respectively. We obtained the multiple linear regression equation: $RPI_{ITCZ} = 12.33 - 1.82\ AI_{EJ} + 1.33\ EEI + 0.94\ SWI$. The correlation coefficient between RPI_{ITCZ} and the original PI_{ITCZ} was 0.82 (Fig. 14a). According to the partial regression coefficients, the reduced area of the EJ in the NSCS and increased strength of the EE contributed significantly to the northward movement of the ITCZ. We also found that the ITCZ moved north at its highest speed at about 1200 UTC on 1 October (Fig. 14a) and the EJ in the NSCS decreased during the same period, but the EE and southwesterly winds strengthened preceding the northward movement of the ITCZ by 6 and 12 hours, respectively (Fig. 14b).

6. Summary and discussion

The ITCZ can cause heavy rainfall over the SCS as it moves north in the autumn. In this paper, we investigated

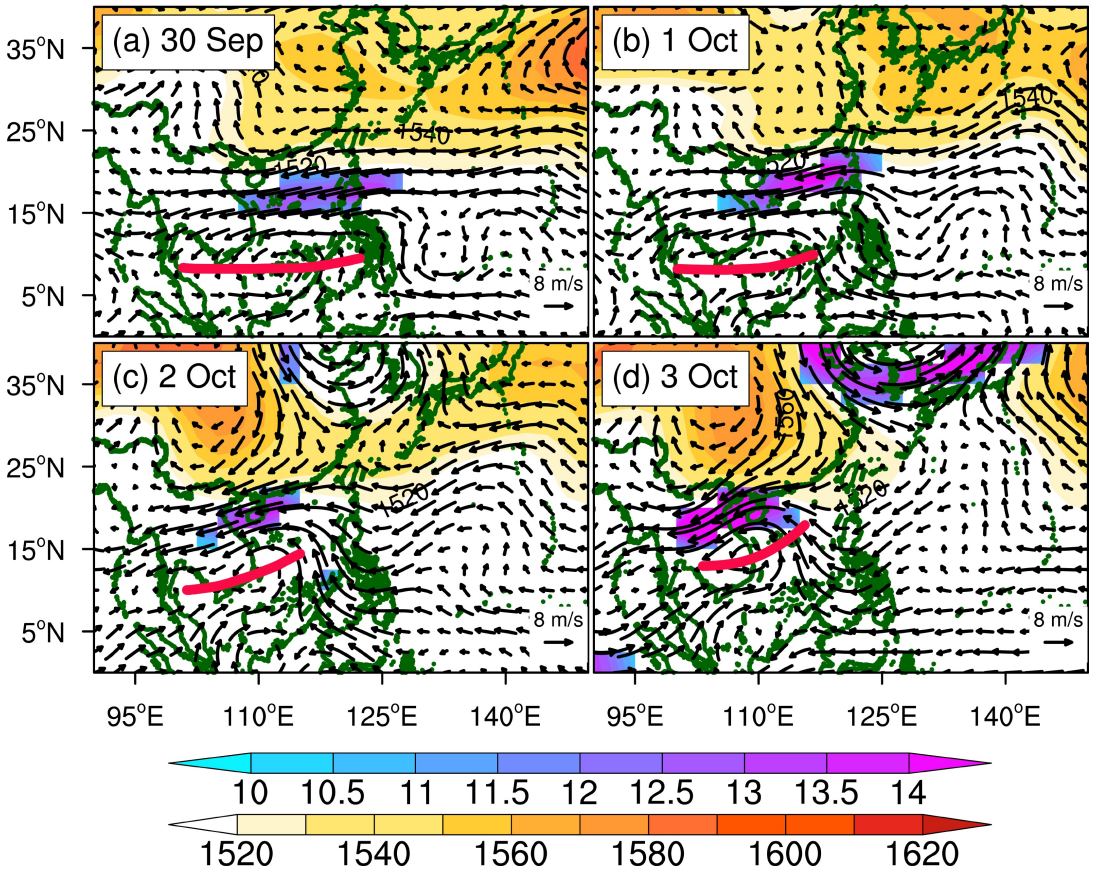

Fig. 13. The 850 hPa geopotential height (warm shading, only values greater than 1520 are shown; units: gpm), the jet (cold shading, only values greater than 10 are shown; units: m s^{-1}), and wind (arrows; units: m s^{-1}). (a)–(d) are 30 September and 1–3 October 2010, respectively. The red line represents the distribution of P_{ITCZ} in the SCS.

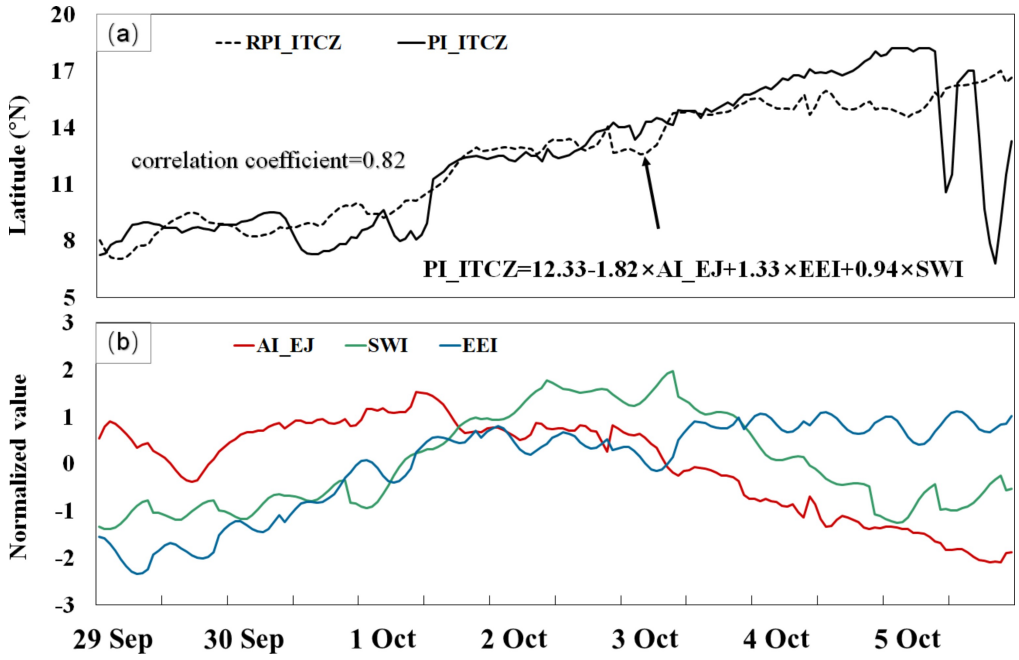

Fig. 14. Time series of (a) the original PI_{ITCZ} (solid) and multiple regression analysis (dashed), and the (b) AI_{EJ} (red), EEI (blue), and SWI (green).

one non-TC heavy rainfall event that occurred between 29 September and 5 October 2010 and analyzed the factors that facilitated the northward movement of the ITCZ.

The appropriate position for the ITCZ to influence the NSCS was 12°N. As the ITCZ moved north to around 12°N, it transported moisture from the Bay of Bengal into the NSCS, intensified the dynamic field by transporting the positive vorticity both horizontally and vertically, and increased atmospheric instability after converging with the cold air carried by the CH. This set of circumstances provided favorable conditions for the development and maintenance of heavy rainfall.

The rapid northerly movement of the ITCZ was related to the EE, southwesterly winds, and EJ over the NSCS. Multiple linear regression analysis showed that the reduced area of the EJ in the NSCS and the increased strength of the EE were the two most important factors that drove the northward movement of the ITCZ. The strengthening of the EE preceded the rapid northward movement of the ITCZ by six hours. The strengthening of the EE could be attributed to the enhanced area of high pressure on the east side of Australia and the Walker circulation. The decrease in the EJ area in the NSCS was caused mainly by the eastward retreat and merger of the CH and the WPSH. Consequently, the variation of the area of the EJ over the NSCS and the EE may be the indicators that can be used to predict the movement of the ITCZ and heavy rainfall in the NSCS in autumn.

The contributions of different factors to the northward movement of the ITCZ may vary under different scenarios. However, the events associated with the northward movement of the ITCZ between 2008 and 2017 indicate that the impact of the EE and EJ in the NSCS upon the northward movement of ITCZ is well-defined, especially in La Niña years. This differs from our previous understanding of their effects on the ITCZ (i.e., the EE inhibits the development of the ITCZ and the EJ in the NSCS strengthens the ITCZ, Gao et al., 2011). In addition, these events demonstrate that the position where the ITCZ begins to affect the NSCS is about 12°N. Furthermore, in La Niña years, some larger-scale factors (e.g., the Madden-Julian Oscillation) may play important roles in non-TC precipitation over the NSCS caused by the northward movement of the ITCZ. We will consider these additional factors in a future study.

Acknowledgements. The research is supported by the Key Laboratory of South China Sea Meteorological Disaster Prevention and Mitigation of Hainan Province (Grant No. SCSF201906), the National Natural Science Foundation of China (Grant No. 41975008), and the Fundamental Research Funds for the Central Universities (Grant No. 201861003). The authors gratefully acknowledge NASA (https://disc.gsfc.nasa.gov/datasets/TRMM_3B42RT_Daily_7/summary), the NOAA Physical Sciences Laboratory (https://psl.noaa.gov/), the Japan Meteorological Agency (http://www.data.jma.go.jp/fcd/yoho/typhoon/position_table/index.html) and the ECMWF (https://climate.copernicus.eu/climate-reanalysis) for providing the data used in this paper.

REFERENCES

Bian, J. P., J. Fang, G. H. Chen, and C. J. Liu, 2018: Circulation features associated with the record-breaking typhoon silence in August 2014. *Adv. Atmos. Sci.*, **35**, 1321–1336, https://doi.org/10.1007/s00376-018-7294-4.

Chang, C. P., P. A. Harr, and H. J. Chen, 2005: Synoptic disturbances over the equatorial South China Sea and western Maritime Continent during boreal winter. *Mon. Wea. Rev.*, **133**, 489–503, https://doi.org/10.1175/MWR-2868.1.

Chen, J., W. L. Liang, A. N. Gao, W. B. Chen, and W. Tang, 2015: Analysis on features of monsoon trough rainstorms in South China. *Journal of Tropical Meteorology*, **31**, 536–548, https://doi.org/10.16032/j.issn.1004-4965.2015.04.011. (in Chinese with English abstract)

Chen, J. M., T. Li, and C. F. Shih, 2010: Tropical Cyclone- and Monsoon-Induced rainfall variability in Taiwan. *J. Climate*, **23**, 4107–4120, https://doi.org/10.1175/2010JCLI3355.1.

Chen, M., and Y. G. Zheng, 2004: Vorticity budget investigation of a simulated long-lived mesoscale vortex in South China. *Adv. Atmos. Sci.*, **21**, 928–940, https://doi.org/10.1007/BF02915595.

Chiodi, A. M., and D. E. Harrison, 2015: Equatorial Pacific easterly wind surges and the onset of La Niña Events. *J. Climate*, **28**, 776–792, https://doi.org/10.1175/JCLI-D-14-00227.1.

Fasullo, J., and P. J. Webster, 2003: A hydrological definition of Indian monsoon onset and withdrawal. *J. Climate*, **16**, 3200–3211, https://doi.org/10.1175/1520-0442(2003)016<3200a:AHDOIM>2.0.CO;2.

Feng, W., S. H. Fu, and F. Z. Zhao, 2015: Circulation of extreme rainstorm and its anomalous characteristics during post-flood period of the last decade in Hainan island. *Meteorological Monthly*, **41**, 143–152, https://doi.org/10.7519/j.issn.1000-0526.2015.02.002. (in Chinese with English abstract)

Feng, W., Y. Wu, F. Z. Zhao, and L. L. Zhou, 2017: Comparative analysis of circulation feature and dynamic structure of the rainstorms with different intensity during the autumn flood season in Hainan island. *Journal of the Meteorological Sciences*, **37**, 784–796, https://doi.org/10.3969/2016jms.0077. (in Chinese with English abstract)

Feng, X., R. G. Wu, J. P. Chen, and Z. P. Wen, 2013: Factors for interannual variations of September-October Rainfall in Hainan, China. *J. Climate*, **26**, 8962–8978, https://doi.org/10.1175/JCLI-D-12-00728.1.

Gao, J. Y., J. H. Yu, X. Z. Zhang, and R. Y. Zhang, 2011: On relationship between variation of the monsoon trough intensity in the South China Sea-Western North Pacific and tropical cyclone activities. *Journal of Tropical Meteorology*, **27**, 63–73, https://doi.org/10.3969/j.issn.1004-4965.2011.01.007. (in Chinese with English abstract)

Gu, W., L. Wang, W. J. Li, L. J. Chen, and C. H. Sun, 2015: Influence of the tropical Pacific east-west thermal contrast on the autumn precipitation in South China. *International Journal of Climatology*, **35**, 1543–1555, https://doi.org/10.1002/joc.4075.

Hersbach, H., and Coauthors, 2020: The ERA5 global reanalysis. *Quart. J. Roy. Meteor. Soc.*, **146**, 1999–2049, https://doi.org/10.1002/qj.3803.

Hu, P., W. Chen, S. F. Chen, Y. Y. Liu, R. P. Huang, and S. R. Dong, 2020: Relationship between the South China Sea summer monsoon withdrawal and September-October rainfall

over southern China. *Climate Dyn.*, **54**, 713–726, https://doi.org/10.1007/s00382-019-05026-2.

Hu, Y. Y., D. W. Li, and J. P. Liu, 2007: Abrupt seasonal variation of the ITCZ and the Hadley circulation. *Geophys. Res. Lett.*, **34**, L18814, https://doi.org/10.1029/2007GL030950.

Huang, B. Y., and Coauthors, 2017: Extended Reconstructed Sea Surface Temperature, version 5 (ERSSTv5): Upgrades, validations, and intercomparisons. *J. Climate*, **30**, 8179–8205, https://doi.org/10.1175/JCLI-D-16-0836.1.

Huffman, G. J., R. F. Adler, D. T. Bolvin, and E. J. Nelkin, 2010: The TRMM multi-satellite precipitation analysis (TMPA). *Satellite Rainfall Applications for Surface Hydrology*, M. Gebremichael and F. Hossain, Eds., Springer, 3–22, https://doi.org/10.1007/978-90-481-2915-7_1.

Jiang, H. Y., and E. J. Zipser, 2010: Contribution of tropical cyclones to the global precipitation from eight seasons of TRMM data: Regional, Seasonal, and Interannual Variations. *J. Climate*, **23**, 1526–1543, https://doi.org/10.1175/2009JCLI3303.1.

Kalnay, E., and Coauthors, 1996: The NCEP/NCAR 40-year reanalysis project. *Bull. Amer. Meteor. Soc.*, **77**, 437–472, https://doi.org/10.1175/1520-0477(1996)077<0437:TNYRP>2.0.CO;2.

Lander, M. A., 1996: Specific tropical cyclone track types and unusual tropical cyclone motions associated with a reverse-oriented monsoon trough in the western North Pacific. *Wea. Forecasting*, **11**, 170–186, https://doi.org/10.1175/1520-0434(1996)011<0170:STCTTA>2.0.CO;2.

Li, R., S. Y. Wang, R. R. Gillies, B. M. Buckley, L. H. Truong, and C. Cho, 2015: Decadal oscillation of autumn precipitation in Central Vietnam modulated by the East Pacific-North Pacific (EP-NP) teleconnection. *Environmental Research Letters*, **10**, 024008, https://doi.org/10.1088/1748-9326/10/2/024008.

Li, T., and J. H. Ju, 2013: Comparison of climate features between the Southwest Summer Monsoon of the Bay of Bengal and the South China Sea Summer Monsoon. *Chinese Journal of Geophysics*, **56**, 27–37, https://doi.org/10.6038/cjg20130103. (in Chinese with English abstract)

Li, W., D. Wang, T. Lei, and H. Wang, 2009: Convective and stratiform rainfall and heating associated with the summer monsoon over the South China Sea based on TRMM data. *Theor. Appl. Climatol.*, **95**, 157–163, https://doi.org/10.1007/s00704-007-0372-7.

Li, Y., R. Y. Lu, and J. H. He, 2006: Tropical large-scale atmospheric circulation and sea surface temperature corresponding to autumn precipitation in Hainan island. *Chinese Journal of Atmospheric Sciences*, **30**, 1034–1042, https://doi.org/10.3878/j.issn.1006-9895.2006.05.29. (in Chinese with English abstract)

Liebmann, B., and C. A. Smith, 1996: Description of a complete (interpolated) outgoing longwave radiation dataset. *Bull. Amer. Meteor. Soc.*, **77**, 1275–1277.

Liu, L. J., W. Feng, and D. M. Chen, 2010: The diagnostic analysis of heavy rainstorm associated with low-level easterly jet in Hainan province. *Torrential Rain and Disasters*, **29**, 328–333, https://doi.org/10.3969/j.issn.1004-9045.2010.04.005. (in Chinese with English abstract)

Liu, Q., L. F. Sheng, Z. Q. Cao, Y. N. Diao, W. C. Wang, and Y. Zhou, 2017: Dual effects of the winter monsoon on haze-fog variations in eastern China. *J. Geophys. Res.*, **122**, 5857–5869, https://doi.org/10.1002/2016JD026296.

Magnusdottir, G., and C. C. Wang, 2008: Intertropical convergence zones during the active season in daily data. *J. Atmos. Sci.*, **65**, 2425–2436, https://doi.org/10.1175/2007JAS2518.1.

Meenu, S., K. Rajeev, K. Parameswaran, and C. S. Raju, 2007: Characteristics of the double intertropical convergence zone over the tropical Indian Ocean. *J. Geophys. Res.*, **112**, D11106, https://doi.org/10.1029/2006JD007950.

Nguyen, L. T., and J. Molinari, 2015: Simulation of the downshear reformation of a tropical cyclone. *J. Atmos. Sci.*, **72**, 4529–4551, https://doi.org/10.1175/JAS-D-15-0036.1.

Niu, N., and J. P. Li, 2008: Interannual variability of autumn precipitation over South China and its relation to atmospheric circulation and SST anomalies. *Adv. Atmos. Sci.*, **25**, 117–125, https://doi.org/10.1007/s00376-008-0117-2.

Ren, F. M., G. X. Wu, W. J. Dong, X. L. Wang, Y. M. Wang, W. X. Ai, and W. J. Li, 2006: Changes in tropical cyclone precipitation over China. *Geophys. Res. Lett.*, **33**, L20702, https://doi.org/10.1029/2006GL027951.

Richter, I., S. P. Xie, Y. Morioka, T. Doi, B. Taguchi, and S. Behera, 2017: Phase locking of equatorial Atlantic variability through the seasonal migration of the ITCZ. *Climate Dyn.*, **48**, 3615–3629, https://doi.org/10.1007/s00382-016-3289-y.

Shang, S. L., and Coauthors, 2008: Changes of temperature and bio-optical properties in the South China Sea in response to Typhoon Lingling, 2001. *Geophys. Res. Lett.*, **35**, L10602, https://doi.org/10.1029/2008GL033502.

Sreekala, P. P., S. V. Bhaskara Rao, M. S. Arunachalam, and C. Harikiran, 2014: A study on the decreasing trend in tropical easterly jet stream (TEJ) and its impact on Indian summer monsoon rainfall. *Theor. Appl. Climatol.*, **118**, 107–114, https://doi.org/10.1007/s00704-013-1049-z.

Srock, A. F., and L. F. Bosart, 2009: Heavy Precipitation associated with southern Appalachian cold-air damming and Carolina coastal frontogenesis in advance of weak landfalling tropical storm Marco (1990). *Mon. Wea. Rev.*, **137**, 2448–2470, https://doi.org/10.1175/2009MWR2819.1.

Wang, C. C., and G. Magnusdottir, 2006: The ITCZ in the central and eastern Pacific on synoptic time scales. *Mon. Wea. Rev.*, **134**, 1405–1421, https://doi.org/10.1175/MWR3130.1.

Wang, S. Y. S., and Coauthors, 2015: Changes in the autumn precipitation and tropical cyclone activity over Central Vietnam and its East Sea. *Vietnam Journal of Earth Sciences*, **36**, 489–496, https://doi.org/10.15625/0866-7187/36/4/6437.

Wei, D. N., J. L. Sun, and Y. P. Li, 2008: Analysis of the anomalous strength and location of the ITCZ affecting the formation of northern Pacific typhoons. *Journal of Ocean University of China*, **7**, 124–130, https://doi.org/10.1007/s11802-008-0124-z.

Wu, Y. J., S. G. Wu, and P. M. Zhai, 2007: The impact of tropical cyclones on Hainan Island's extreme and total precipitation. *International Journal of Climatology*, **27**, 1059–1064, https://doi.org/10.1002/joc.1464.

Xiao, C., W. H. Yuan, J. Li, and R. C. Yu, 2013: Preliminary study of autumn rain in the South China Sea. *Climatic and Environmental Research*, **18**, 693–700, https://doi.org/10.3878/j.issn.1006-9585.2013.12163. (in Chinese with English abstract)

Xie, S. P., Q. H. Peng, Y. Kamae, X. T. Zheng, H. Tokinaga, and D. X. Wang, 2018: Eastern Pacific ITCZ dipole and ENSO

diversity. *J. Climate*, **31**, 4449–4462, https://doi.org/10.1175/JCLI-D-17-0905.1.

Yen, M. C., T. C. Chen, H. L. Hu, R. Y. Tzeng, D. T. Dinh, T. T. T. Nguyen, and C. J. Wong, 2011: Interannual variation of the fall rainfall in central Vietnam. *J. Meteor. Soc. Japan*, **89A**, 259–270, https://doi.org/10.2151/jmsj.2011-A16.

Yokoi, S., and J. Matsumoto, 2008: Collaborative effects of cold surge and tropical depression-type disturbance on heavy rainfall in central Vietnam. *Mon. Wea. Rev.*, **136**, 3275–3287, https://doi.org/10.1175/2008MWR2456.1.

Yokoi, S., T. Satomura, and J. Matsumoto, 2007: Climatological characteristics of the intraseasonal variation of precipitation over the Indochina Peninsula. *J. Climate*, **20**, 5301–5315, https://doi.org/10.1175/2007JCLI1357.1.

Zhang, S. P., and S. C. Jiang, 2001: Possible influences of ITCZ in Asian monsoon regions on rainy season anomaly of North China. *Adv. Atmos. Sci.*, **05**, 1018–1028, https://doi.org/10.1007/BF03403520.

Zhao, F. Z., F. Wang, and W. Feng, 2011: Preliminary study on circulation characteristics and mechanism of rainstorm in autumn of Hainan island. *Chinese Journal of Tropical Agriculture*, **31**, 50–57, https://doi.org/10.3969/j.issn.1009-2196.2011.05.012. (in Chinese with English abstract)

Zhao, S. X., N. F. Bei, and J. H. Sun, 2007: Mesoscale analysis of a heavy rainfall event over Hong Kong during a pre-rainy season in South China. *Adv. Atmos. Sci.*, **24**, 555–572, https://doi.org/10.1007/s00376-007-0555-2.

Zhou, B. T., and X. Cui, 2011: Sea surface temperature east of Australia: A predictor of tropical cyclone frequency over the western North Pacific? *Chinese Science Bulletin*, **56**, 196–201, https://doi.org/10.1007/s11434-010-4157-5.